Supporting Information

Synergistic Functionalization and Descriptor-Driven Screening of MBene Electrocatalysts for High-Performance Li-S Batteries

Chen Yang[1], Dongyue Gao[1,*], Shuaipeng Mao[1], Junxia Li[1], Yi Fang[1], Yang Huang[1], Chengchun Tang[1], Zhonglu Guo[1,*]

[1]*Hebei Key Laboratory of Boron Nitride Micro and Nano Materials*, *School of Materials Science and Engineering, Hebei University of Technology, Tianjin 300130, China*

*Correspondence and requests for materials should be addressed to D. Y. Gao or Z. L. Guo: gaodongyue9@163.com, zlguo@hebut.edu.cn.

Convergence Tests regarding the supercell size and vacuum thickness

Avoiding periodic image interactions is essential to ensure the reliability of simulation parameters. We therefore performed systematic tests by expanding the supercell size and increasing the vacuum layer thickness for the stable adsorption configurations of polysulfides on $Mo_2B_2O_2$. First, using a vacuum layer of 20 Å, we examined the effect of supercell size by expanding it from 3×3×1 to 4×4×1. As shown in Fig. S1 and Table S1, after expanding the supercell, the changes in adsorption energies for all polysulfides were less than 0.2 eV compared to the previous results, and the variations in diffusion barriers and decomposition barriers were also minimal. This indicates that periodic image interactions are negligible under the 3×3×1 supercell. Next, we tested the influence of vacuum layer thickness. The diffusion and decomposition barriers are primarily determined by the breaking and forming of local chemical bonds, with vacuum layer thickness exerting negligible influence on such structural changes. Furthermore, since the vacuum layer mainly impacts interactions along the c-axis direction, its effect if minimal on the adsorption energies of long-chain lithium polysulfides would likewise be insignificant for short-chain lithium polysulfides. Therefore, we only calculated adsorption energies for long-chain polysulfides (Li_2S_8 and Li_2S_6). The results show that for the 3×3×1 supercell, increasing the vacuum thickness from 20 Å to 25 Å leads to changes in adsorption energies of less than 0.1 eV. Therefore, the 20 Å vacuum thickness used throughout our study is fully converged.

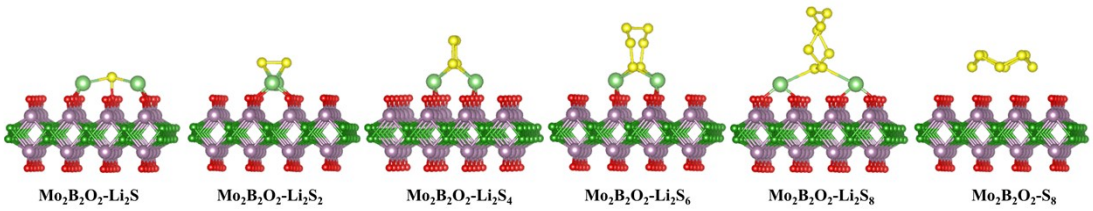

Fig. S1 Side view of $Mo_2B_2O_2$ adsorbing S_8/LiPSs in a 4×4×1 supercell.

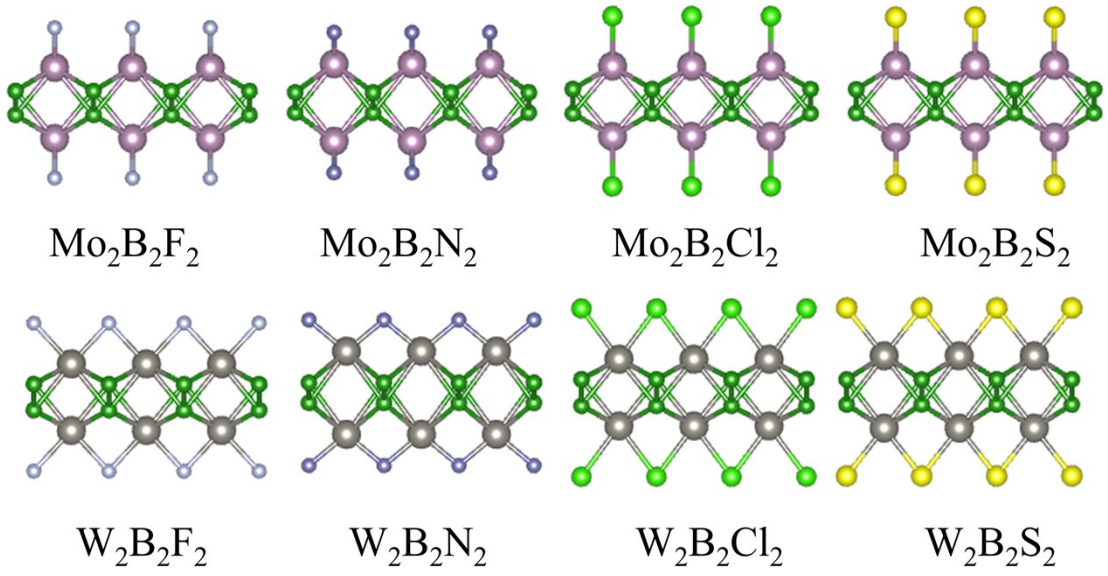

Fig. S2 Side view of (a) $Mo_2B_2T_2$ and (b) $W_2B_2T_2$ (T =F, N, Cl, S).

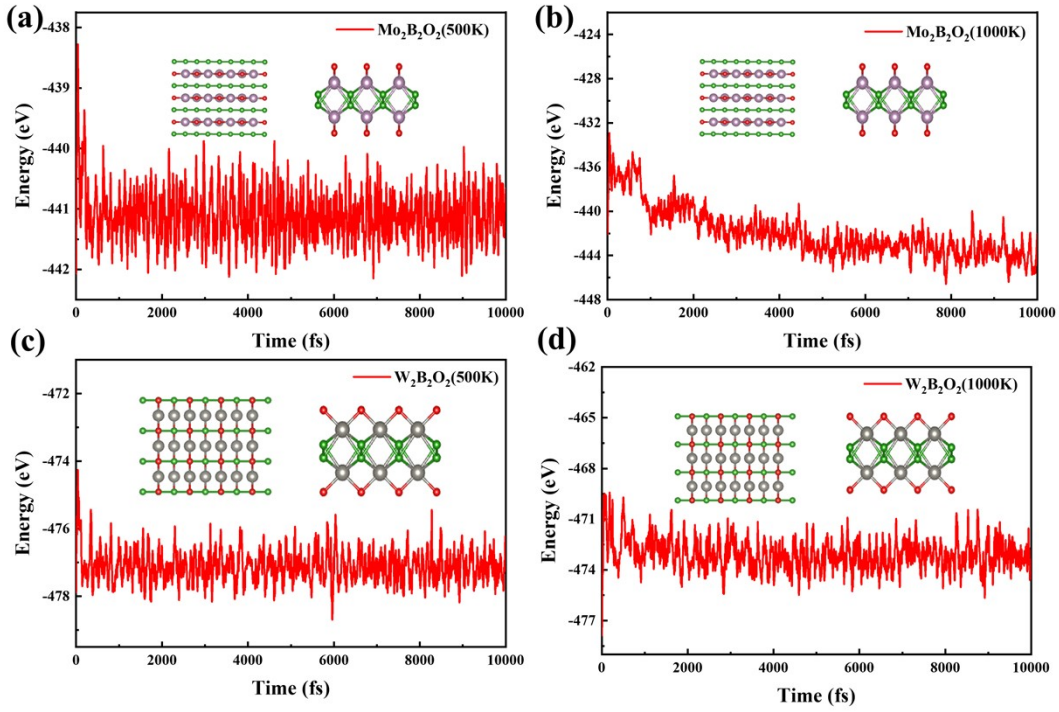

Fig. S3 The AIMD simulation result of $Mo_2B_2O_2$ and $W_2B_2O_2$ at 500 K and 1000K

for 10 ps.

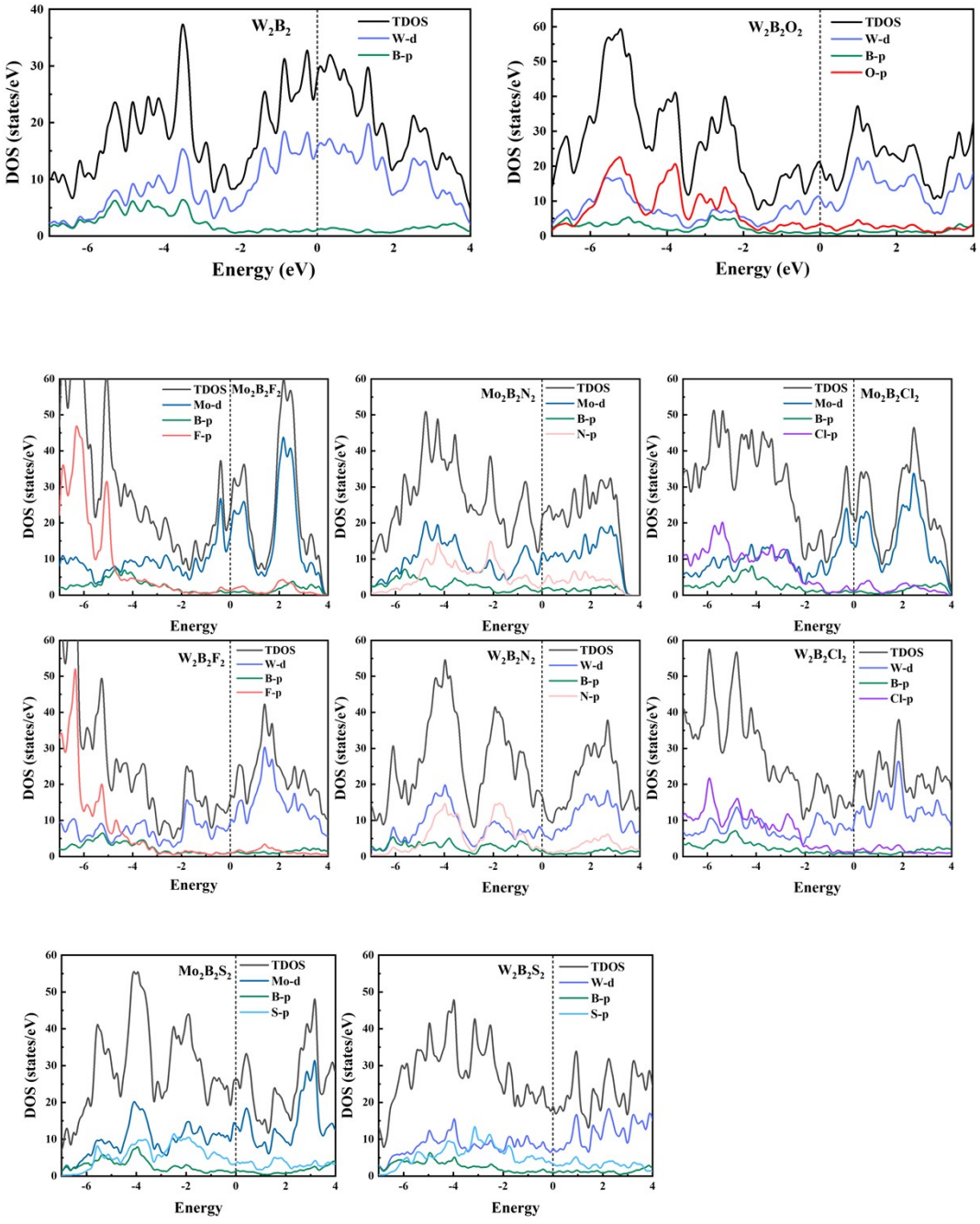

Fig. S4 The total and partial density of states (DOS) of Mo_2B_2, $Mo_2B_2T_2$ and $W_2B_2T_2$ (T =O, F, N, Cl, S) configurations.

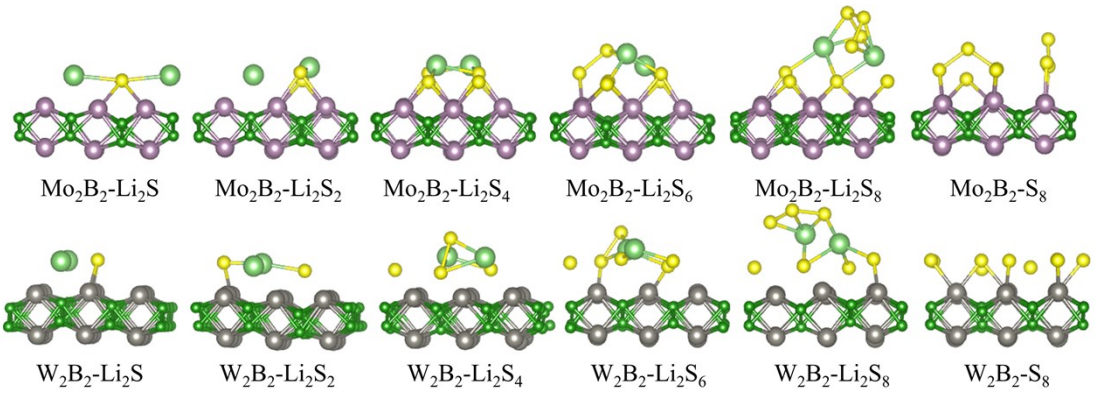

Fig. S5 Adsorption configurations of S_8 and Li_2S_n on the surface of (a) Mo2B2 and (b) W_2B_2.

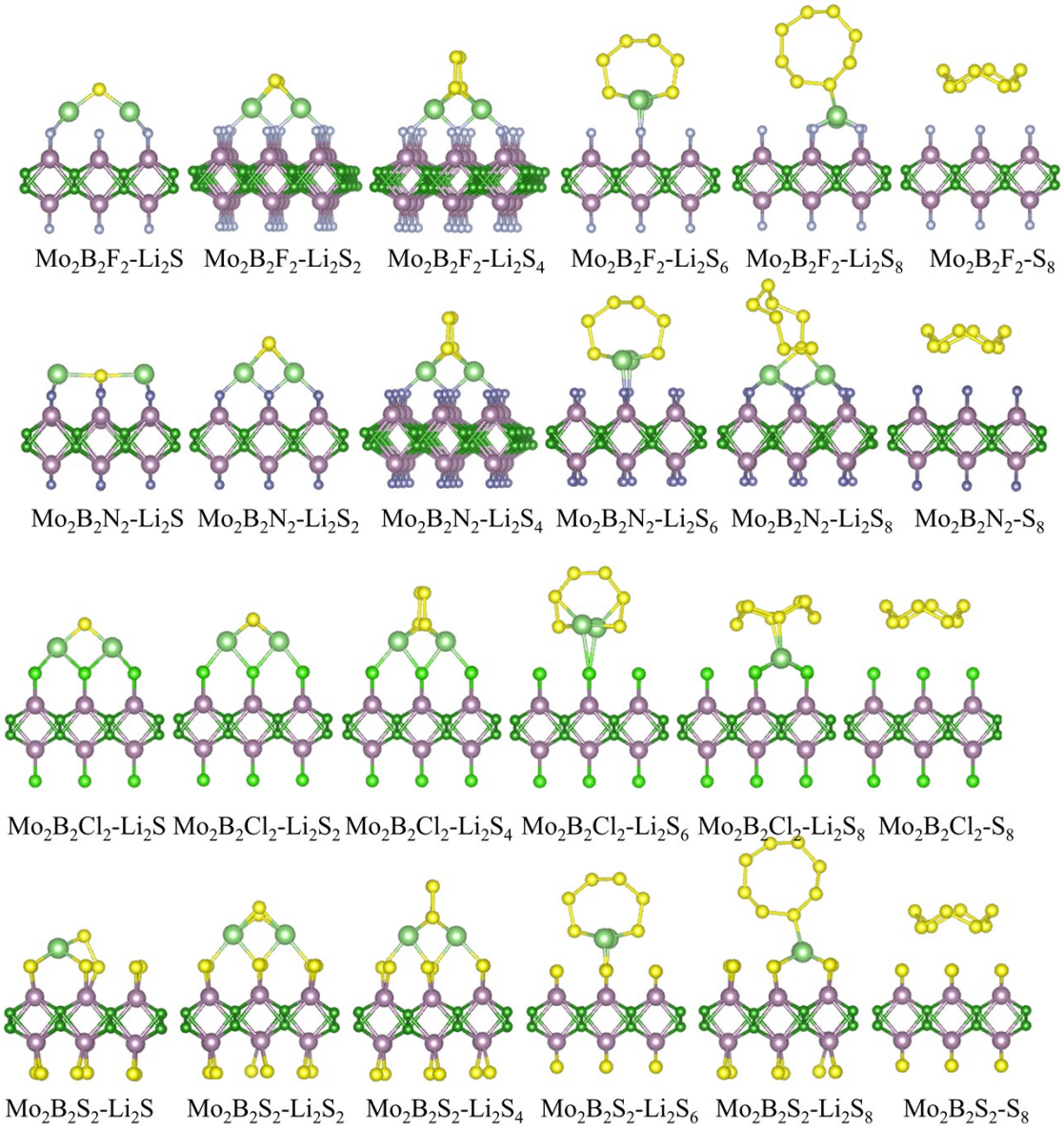

Fig. S6 Adsorption configurations of S_8 and Li_2S_n on the surface of $Mo_2B_2T_2$ (T =F, N, Cl, S).

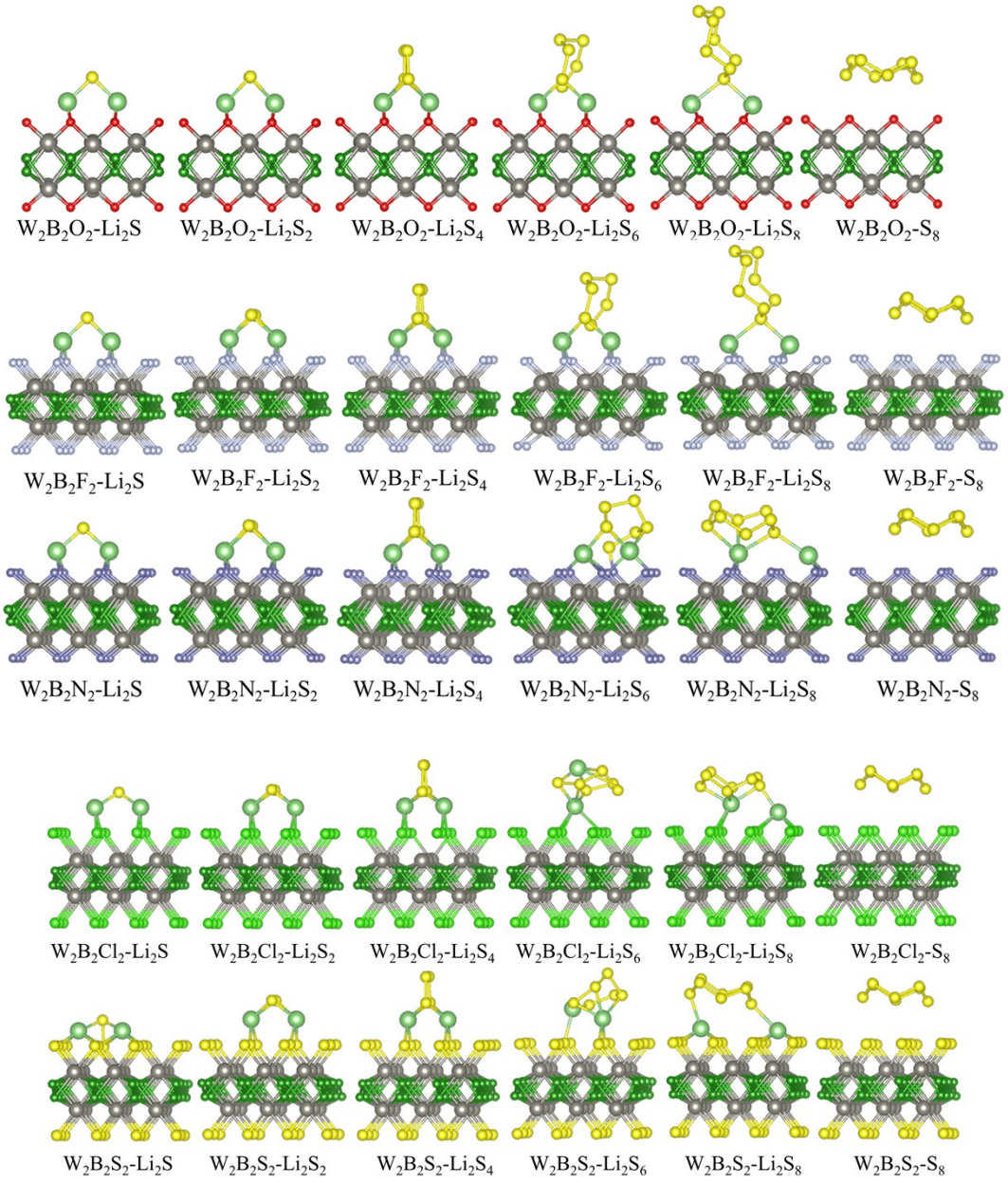

Fig. S7 Adsorption configurations of S_8 and Li_2S_n on the surface of $W_2B_2T_2$ (T =O, F, N, Cl, S).

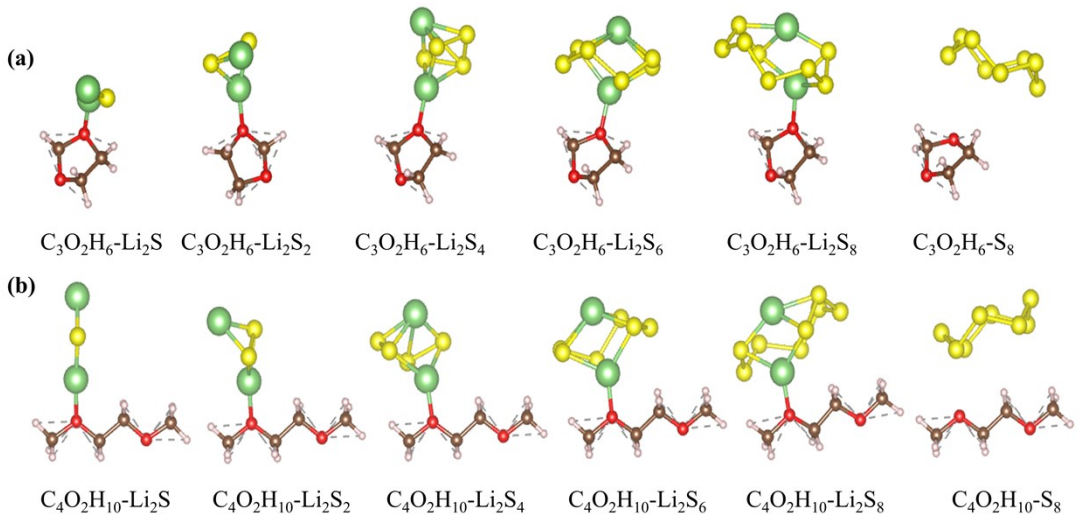

Fig. S8 The stable adsorption configurations of 1,3-dioxolane (DOL) and 1,2-dimethoxyethane (DME) solvent molecules for S_8/Li_2S_n.

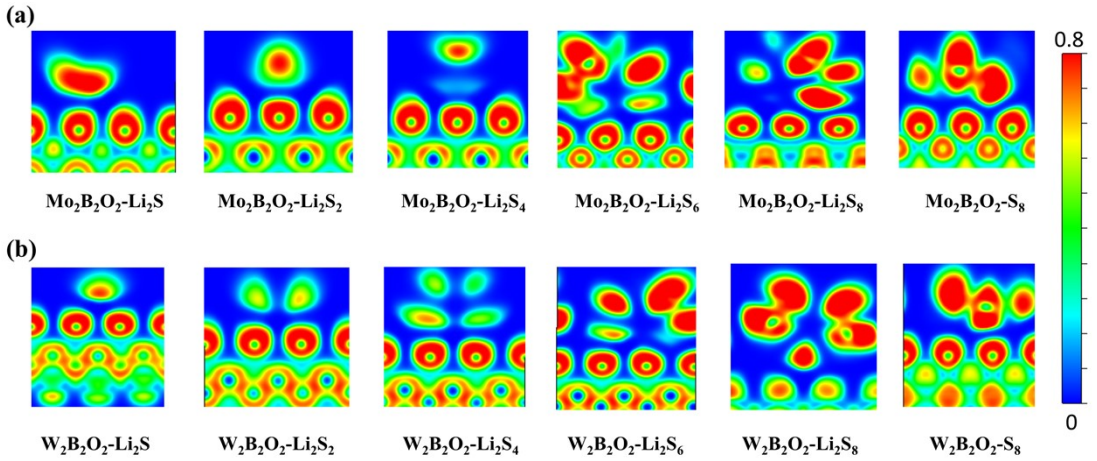

Fig. S9 Electron localization function (ELF) of S_8/LiPSs and functionalized MBenes.

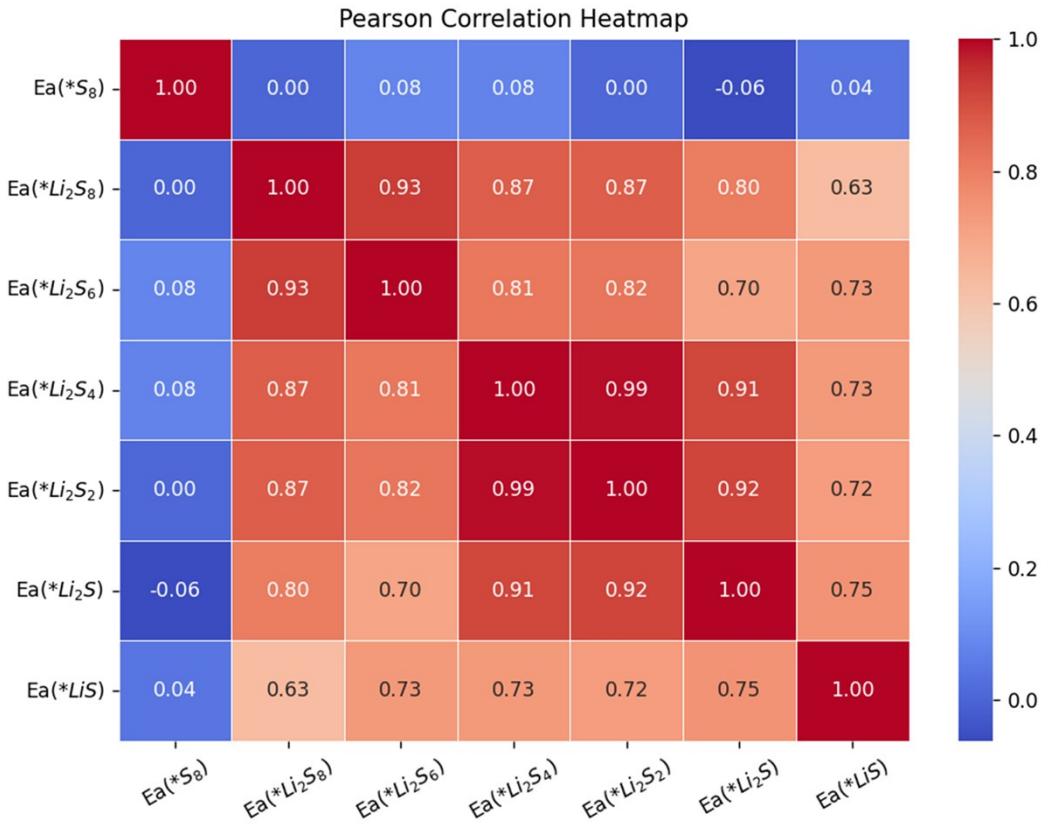

Fig. S10 Heatmap of the Pearson correlation matrix for MBene and SACs adsorption energy of S_8/LiPSs descriptors.

Table S1. Effect of Supercell Size and Vacuum Layer Thickness on Adsorption Energies and Diffusion/Decomposition Barriers

$Mo_2B_2O_2$	S_8	Li_2S_8	Li_2S_6	Li_2S_4	Li_2S_2	Li_2S	E_{diff}	E_{dec}
331(20 Å)	-1.37	-5.04	-3.02	-4.27	-4.23	-5.44	0.09	0.436
441(20 Å)	-1.27	-4.98	-2.96	-4.11	-4.41	-5.55	0.06	0.462
25 Å (331)		-4.91	-3.03					

Table S2. Average Li-intercalation voltage of $Li_xMo_2B_2O_2$

	$E(Li_xMo_2B_2O_2)$	$E(Mo_2B_2O_2)$	E(Li)	V_{avg}
$Li_1Mo_2B_2O_2$	-462.2 eV	-457.1 eV	-2.8 eV	2.3 V
$Li_5Mo_2B_2O_2$	-480.4 eV	-457.1 eV	-2.8 eV	1.86 V
$Li_9Mo_2B_2O_2$	-494.5 eV	-457.1 eV	-2.8 eV	1.36 V

Table S3. The adsorption energies of $Mo/W_2B_2T_2$(T = O, F, N, Cl, S) to S_8/LiPSs.

Structures	E_a/Li_2S (eV)	E_a/Li_2S_2 (eV)	E_a/Li_2S_4 (eV)	E_a/Li_2S_6 (eV)	E_a/Li_2S_8 (eV)	E_a/S_8 (eV)
$Mo_2B_2O_2$	-5.44	-4.233	-4.274	-3.023	-5.045	-1.365
$Mo_2B_2F_2$	-2.022	-2.252	-1.977	-1.149	-1.876	-0.93
$Mo_2B_2N_2$	-6.037	-3.419	-3.35	-2.328	-4.111	-1.635
$Mo_2B_2Cl_2$	-1.222	-1.206	-0.621	-0.574	-0.691	-0.669
$Mo_2B_2S_2$	-3.893	-2.371	-2.026	-1.532	-2.256	-1.662
$W_2B_2O_2$	-3.297	-3.510	-3.360	-2.413	-3.806	-1.015
$W_2B_2F_2$	-2.262	-2.190	-1.835	-3.211	-5.455	-1.023
$W_2B_2N_2$	-3.344	-3.633	-3.549	-4.509	-4.759	-1.257
$W_2B_2Cl_2$	-1.334	-1.287	-0.692	-1.106	-0.930	-0.874
$W_2B_2S_2$	-3.136	-1.863	-1.419	-1.255	-2.096	-0.94

Table S4. The Gibbs free-energy change of each reaction for the discharging process in LiSBs.

Structures	ΔG1/(eV)	ΔG2/(eV)	ΔG3/(eV)	ΔG4/(eV)	ΔG5/(eV)
$Mo_2B_2O_2$	-5.713	1.478	-1.215	0.748	-0.382
$Mo_2B_2F_2$	-2.980	0.183	-0.793	0.434	1.055
$Mo_2B_2N_2$	-4.510	1.240	-0.987	0.638	-1.792
$Mo_2B_2Cl_2$	-2.056	-0.426	-0.012	0.123	0.810
$Mo_2B_2S_2$	-2.627	0.180	-0.459	0.363	-0.697
$W_2B_2O_2$	-4.824	0.850	-0.912	0.559	1.038
$W_2B_2F_2$	-6.465	1.701	1.411	0.353	0.753

$W_2B_2N_2$	-5.536	-0.293	0.995	0.624	1.114
$W_2B_2Cl_2$	-2.089	-0.720	0.450	0.114	0.777
$W_2B_2S_2$	-3.189	0.298	-0.129	0.263	-0.447

Table S5. The adsorption energies for the reduction of Li_2S_2 to Li_2S with two different reaction pathways.

Structures	**E_a(LiS)/eV**	**E_a(Li_3S_2)/eV**
$Mo_2B_2O_2$	-4.642	-6.608
$Mo_2B_2F_2$	-0.939	-4.591
$Mo_2B_2N_2$	-6.727	-4.745
$Mo_2B_2Cl_2$	-1.251	-3.609
$Mo_2B_2S_2$	-3.988	-4.756
$W_2B_2O_2$	-3.266	-6.226
$W_2B_2F_2$	-1.315	-3.025
$W_2B_2N_2$	-5.504	-6.185
$W_2B_2Cl_2$	-1.264	-3.522
$W_2B_2S_2$	-0.992	-3.183